Investigating the (Poly)Radicaloid Nature of Real-World Organic Compounds with DFT-Based Methods

Investigating the (poly)radicaloid nature of real-world organic compounds with DFT-based methods

G. Salvitti[a,b], F. Negri[b,c],
A.J. Pérez-Jiménez[a], E. San-Fabián[a],
D. Casanova[d,e], and J. C. Sancho-García[a*]

[a] Department of Physical Chemistry,
University of Alicante,
E-03080 Alicante, Spain

[b] Dipartimento di Chimica "Giacomo Ciamician",
Università di Bologna,
IT-40126 Bologna, Italy

[c] INSTM UdR Bologna, Italy

[d] Donostia International Physics Center (DIPC),
E-20018 Donostia, Spain

[e] IKERBASQUE,
Basque Foundation for Science,
E-48013 Bilbao, Spain

[*]E-mail: jc.sancho@ua.es

Abstract

Recent advances in the synthesis of stable organic (open-shell) polyradicaloids have opened their application as active compounds for emerging technologies. These systems typically exhibit small energy differences between states with different spin multiplicities, which are intrinsically difficult to calculate by theoretical methods. We thus apply here some DFT-based variants (FT-DFT, SF-DFT, and SF-TDDFT) on a test set of large and real-world molecules, as test systems for which such energy differences are experimentally available, also comparing systematically with RAS-SF results to infer if shortcomings of previous DFT applications are corrected. Additionally, we explore the spin-spin contribution to the ZFS tensor, of high interest for EPR spectroscopy, and derive the spatial extent of the corresponding (photoexcited) triplet state.

Key words: organic (poly)radicals, low- and high-spin states, finite-temperature DFT, spin-flip (TD)DFT, ZFS tensor.

1 Introduction

Studying the (poly)radical character of organic molecules is a long-standing field of research due to the many envisioned applications of these compounds.[1,2] Recent experimental developments, in ultrahigh-vacuum surfaces or using non-standard synthetic routes, have propelled the synthesis of highly challenging species including classically studied carbon-rich radicals[3] like triangulenes,[4] graphene nanoribbons with zigzag edges,[5,6] kekulenes,[7] long acenes,[8,9] cyclic nanobelts,[10,11] etc. All these systems share a complicated electronic structure, with (near-)degenerated orbitals lying within the gap between occupied and virtual ones, leading to small exchange interactions and thus close in energy low- (e.g. singlet or doublet) and high-spin (e.g. triplet or quartet) many-body states.[12] Furthermore, C-based magnetism is gaining attention for nanographene fragments since long time ago,[13] and it has been recently demonstrated for well-defined geometrical C-based structures, like those arising from planar conjugated hydrocarbons, how to anticipate the spin multiplicity and energy ordering of the corresponding states,[14] thus complementing the Ovchinnikov's rule[15] and the Lieb theorem.[16] However, for more general situations, one should rely on robust, accurate, and cost-effective theoretical methods, which is still a difficult task not exempted from computational limitations, especially for large systems.[17]

On the other hand, the application of standard Density Functional Theory (DFT) methods to these (poly)radical systems is known to be affected by some pitfalls and/or artifacts: the intrinsic one-determinantal nature of Kohn-Sham (KS) DFT precludes to deal with orbital degeneracies, thus neglecting non-dynamical or static correlation effects, and the use of a Broken-

Symmetry (BS) solution for open-shell systems introduces spin-contamination (also scaling with size[18]) issues mostly affecting the energy of the low-spin solution.[19] This situation has historically prompted the development of non-standard methods able to cope with these subtle electronic effects, namely based on the two-body on-top pair density[20–29] with a revisited interest nowadays,[30–33] the balanced coupling of *ab initio* and density functional expressions,[34–37] the use of natural orbitals[38–40] or the specific *ensemble* of pure spin states,[41–43] to name just a few of the existing non-standard methods. Another possible route is the use of fractional spin[44] or orbital occupation,[45,46] mimicking the situation when multiconfigurational *ab initio* methods are instead employed, or spin-flip techniques,[47–49] describing target states from a high-spin reference state.

To further explore (*vide infra*) the applicability and accuracy of modern DFT variants, in the search for the best trade-off between accuracy and computational cost, we have chosen a set of large (and real-world) organic radical compounds recently synthesized and crystallized with diverse structural motifs (see Figure 1). Note that for all of the systems selected, their stability has allowed the original authors to perform experimental measurements such as Electron Spin Resonance (ESR) or Superconducting QUantum Interference Device (SQUID), among others, to extract e.g., the energy difference between low- and high-spin states, thus allowing to bracket the accuracy of the theoretical methods employed after the comparison with experimental results. The systems selected here (and their short names used in the following) are: (i) substituted Blatter-like radicals[50,51] (Diradical I and II); (ii) [6]cyclo-para-phenylmethine[52] (6CPPM-Mes); (iii) [n]cyclo-para-biphenylmethines[53] ([n]CPBM-Ant) with $n = 3 - 6$; (iv) ethynylene-

bridged fluorenyl macrocycle[54] (MC-F3A3); and (v) cyclopenta-ring-fused oligo(m-phenylene) macrocyclic[55] (8MC). Note that the DFT-based results will also be compared with those from the Restricted-Active-Space Spin-Flip (RAS-SF) method,[56] to bracket their accuracy also for magnitudes for which experimental results are not available.

2 Theoretical Methods

2.1 The FT-DFT method

The Finite-Temperature DFT (FT-DFT) method relies on the fractional occupation of molecular orbitals induced by (near-)degeneracy effects, with the associated density written as:

$$\rho(\mathbf{r}) = \sum_{i}^{\infty} f_i |\phi_i(\mathbf{r})|^2, \tag{1}$$

where $\phi_i(\mathbf{r})$ is a molecular spin-orbital and f_i its fractional electron occupation numbers ($0 \leq f_i \leq 1$). The self-consistency of the procedure is achieved by minimizing the Gibbs electronic free energy ($G_{el} = E_{el} - T_{el}S_{el}$) of the system at a fictitious pseudo-temperature (i.e., electronic) called T_{el}, with the f_i values obtained by a Fermi-Dirac distribution around the Fermi level E_F:

$$f_i = \frac{1}{1 + e^{(\epsilon_i - E_F)/\theta}}, \tag{2}$$

depending on $\theta = k_B T_{el}$. The corresponding energy difference between the low-spin (LS) and high-spin (HS) solutions can be calculated after imposing the desired spin multiplicity, $\Delta E(\mathrm{LS} - \mathrm{HS}) = E(\mathrm{LS}) - E(\mathrm{HS})$, with $\Delta E(\mathrm{LS} - \mathrm{HS}) < 0$ indicating a favoured low-spin ground-state (antiferromagnetic). Note the similarities between this method and the Thermally-Assisted-Occupation (TAO) DFT method of Chai *et al.*[46,57]

2.1.1 Characterization of the radical character

Additionally, the set $\{f_i, \phi_i(\mathbf{r})\}$ can be used to define a density of unpaired electrons, that is the Fractional Orbital Density (FOD)[58,59] as:

$$\rho^{FOD}(\mathbf{r}) = \sum_{i}^{M} (\delta_1 - \delta_2 f_i) \, |\phi_i(\mathbf{r})|^2, \tag{3}$$

where δ_1 and δ_2 are chosen to become $(1, 1)$ if the single-particle energy level (ϵ_i) associated with the orbital ϕ_i is lower than the energy of the Fermi level, E_F, or $(0, -1)$ otherwise. This density also leads upon integration to a measure of the number of strongly correlated electrons, $N_{FOD} = \int \rho^{FOD}(\mathbf{r}) d\mathbf{r}$, which is a concept equivalent to the (linear) metrics introduced by Head-Gordon,[60] typically labelled as N_U and obtained from natural orbital occupation numbers (NOONs), i.e., the eigenvalues of the one-electron reduced density matrix.

Complementarily, the radical character of electronic states can be quantified by means of the radical indices $0 \leq y_i \leq 1$ ($i = 0$, 1, 2, 3). Within the FT-DFT methodology, they can be directly assigned to the electronic occupations above the Fermi level as $y_i = f^{\alpha}_{\mathrm{LUMO}+i} + f^{\beta}_{\mathrm{LUMO}+i}$, with $f^{\sigma}_{\mathrm{LUMO}+i}$ the fractional occupation number of the lowest unocuppied LUMO+i spin-orbital (since approximately $f^{\sigma}_{\mathrm{LUMO}+i} + f^{\sigma}_{\mathrm{HOMO}-i} = 1$). For systems with a significant (poly)radical nature, the indices y_i can be used to estimate their di- or tri- (y_0), tetra- or penta- (y_1), hexa- or hepta- (y_2), and octa- or nonaradical (y_3) character, respectively. Large indices ($y_i \approx 1$) indicate high radical character, while intermediate values are indicative of moderate (poly)radicaloid character. The similarity of these fractional occupation numbers with the NOONs has been recently confirmed for polycyclic aromatic hydrocarbons,[61] as well as the trend between N_{FOD} and global

biradical values arising from experimental measurements.[62,63]

2.2 The SF-DFT method

The Spin-Flip DFT (SF-DFT) method relies on the exchange of the α and β spin blocks of the density on certain user-defined centers, thus generating a Broken-Symmetry (BS) solution after converging the high-spin wavefunction. The energy difference between both considered configurations is given by $\Delta E(\mathrm{BS}-\mathrm{HS}) = E(\mathrm{BS}) - E(\mathrm{HS})$, which can be used as a first approximation to the energy difference between LS and HS solutions. Energy differences between pure spin states can be estimated by the Yamaguchi's procedure:[64–66]

$$\Delta E(\mathrm{LS}-\mathrm{HS}) = \frac{n_S}{\langle \hat{S}^2 \rangle_{\mathrm{HS}} - \langle \hat{S}^2 \rangle_{\mathrm{BS}}} \Delta E(\mathrm{BS}-\mathrm{HS}), \tag{4}$$

where n_S corresponds to the $\langle \hat{S}^2 \rangle$ difference between the ideal spin multiplicities, e.g., $n_S = 2$ for a LS singlet and a HS triplet, $n_S = 3$ for a LS doublet and a HS quartet, etc.

2.3 The SF-TDDFT method

The Spin-Flip Time-Dependent DFT (SF-TDDFT) method is recognized to uniformly describe excited states of single, double, and mixed excitation character in molecular systems,[67] and more specifically in conjugated molecules featuring diradical or (poly)radical character,[68,69] starting from a high-spin (e.g., triplet) reference state. The formalism is based on the (linear response) TDDFT equations for excitation energies:

$$\begin{bmatrix} \mathbf{A} & \mathbf{B} \\ \mathbf{B}^\star & \mathbf{A}^\star \end{bmatrix} \begin{bmatrix} \mathbf{X} \\ \mathbf{Y} \end{bmatrix} = \Omega \begin{bmatrix} \mathbf{1} & \mathbf{0} \\ \mathbf{0} & -\mathbf{1} \end{bmatrix} \begin{bmatrix} \mathbf{X} \\ \mathbf{Y} \end{bmatrix}, \tag{5}$$

with $\mathbf{X}$ ($\mathbf{Y}$) the set of (de-)excitation amplitudes, $\mathbf{A}$ and $\mathbf{B}$ the linear-response matrices, and Ω the excitation energies. In SF-TDDFT, Eq. (5) is solved for the subspace of spin-flip ($\alpha \rightarrow \beta$) operators.[47] For this case, the general expression for $\mathbf{A}$ and $\mathbf{B}$ elements simplify to $A_{i\bar{a},j\bar{b}} = \delta_{ij}\delta_{\bar{a},\bar{b}}\left(\epsilon_{\bar{a}} - \epsilon_i\right) - C_x\left(ij|\bar{a}\bar{b}\right)$ and $B_{i\bar{a},\bar{j}b} = -C_x\left(ib|\bar{a}\bar{j}\right)$, with C_x the weight of exact exchange of the density functional used, i,j (a,b) refer to occupied (virtual) orbitals (the overbar on orbital indices indicates β-spin), ϵ_p is the energy associated to the KS p-spin-orbital, and $(pq|st)$ is the two electron interaction integral given in Mülliken's notation:

$$(pq|st) = \int \phi_p^*(\mathbf{x})\phi_q(\mathbf{x})\frac{1}{|\mathbf{x}-\mathbf{x}'|}\phi_t^*(\mathbf{x}')\phi_s(\mathbf{x}')\mathrm{d}\mathbf{x}\mathrm{d}\mathbf{x}' \tag{6}$$

2.4 The RAS-SF method

Spin-flip methods with single spin-flip excitations[70–72] are not capable to properly describe low-spin states of molecular systems with more than three unpaired electrons, e.g., tetraradicals. This limitation can be overcome through the generalization of the excitation operator to multiple spin-flip excitations, as in the RAS-SF method. In RAS-SF the orbital space of the high-spin reference is split in three subspaces: doubly occupied (RAS1), singly occupied (RAS2), and virtual (RAS3). The eigenstates of the RAS-SF Hamiltonian are obtained as n-spin-flip excitations expanded in terms of the number of holes (electrons) in the doubly (virtual) spaces:

$$\hat{R}^{n\mathrm{SF}} = \hat{r}_0^{n\mathrm{SF}} + \hat{r}_h^{n\mathrm{SF}} + \hat{r}_p^{n\mathrm{SF}} + \hat{r}_{hp}^{n\mathrm{SF}} + \hat{r}_{2h}^{n\mathrm{SF}} + \hat{r}_{2p}^{n\mathrm{SF}} + ..., \tag{7}$$

where $\hat{r}_0^{n\mathrm{SF}}$ performs all possible spin-flip excitations within RAS2 and h and p subindices indicate the number of holes and electrons in RAS1 and

RAS3, respectively.

2.5 Computational details

We use a semi-local (TPSS[73]) and a pair of hybrid[74] (TPSS0 and TPSSHH) exchange-correlation meta-GGA functionals differing in the weight (C_x) of the EXact-eXchange (EXX) introduced (i.e., 0% for TPSS, 25% for TPSS0, and 50% for TPSSHH) for the FT-DFT and SF-DFT calculations reported here. Note that the original FT-DFT method employed the TPSS funcional, which will be respected here, but we will also complementarily explored the dependence of the results with respect to the EXX weight. The electronic temperature (T_{el}) was fixed for the FT-DFT calculations following the recommended expression $T_{el}/K = 5000 + 20000\ C_x$ as a function of the EXX weight C_x.

We use the cost-effective 6-31G** (SF-DFT) and the large def2-TZVP[75] (FT-TPSS) basis sets for those calculations, together with the RIJCOSX technique[76] (with the def2/JK auxiliary basis sets[77]) to reduce the increase in computational cost associated to the TPSS0 and TPSSHH functionals. The plots of the $\rho^{\mathrm{FOD}}(\mathbf{r})$ density were generated by the UCSF Chimera[78] (version 1.12) package. The FT-DFT and SF-DFT calculations were done with the ORCA (version 4.0.1.2) quantum-chemical package[79] employing ultrafine numerical integration grids (i.e., Grid6, NoFinalGrid) in all cases.

The SF-TDDFT calculations employed the collinear approximation as implemented in the GAMESS package,[80] together with the BHHLYP functional[81] and the cost-effective 6-31G* basis set. Note that the use of a functional with a high $C_x = 0.50$ value is recommended for this kind of

calculations,[47,82] and that the accuracy is not expected to vary using another exchange-correlation functional like TPSSHH of PBEHH (both with the same $C_x = 0.50$ value than BHHLYP).[83]

The RAS-SF calculations have been done within the hole and electron approximation, that is including the three first terms in the rhs of Eq. (5) using a ROHF (Restricted Open-Shell) high-spin reference: triplet (Blatter-like diradicals), quartet ([3]CPBM), quintet ([4]CPBM), sextet ([5]CPBM), septet ([6]CPPM and [6]CPBM), and nonet (8MC). Further details can be found at the Supporting Information and elsewhere.[52–55] These calculations have been done with the Q-Chem (version 5.2) program[84] and the 6-31G** basis set.

Finally, the Zero-Field-Splitting (ZFS) calculations were performed with the ωB97X-D functional[85] and the IGLO-II basis set,[86] intended for computing magnetic properties with high accuracy,[87] together with the 'AutoAux' generation procedure for auxiliary basis sets.[88] The ZFS tensor was self-consistently calculated on the basis on spin-Unrestricted Natural Orbitals (UNO)[89] as recommended.[90] The ZFS calculations were done with the ORCA (version 4.0.1.2) quantum-chemical package[79] employing a tight threshold for convergence (i.e., TightSCF) and ultrafine numerical integration grids (i.e., Grid6, NoFinalGrid) in all cases.

3 Results and discussion

3.1 Quantification of the (poly)radicaloid character.

First, we aim to evaluate the extent of the radical character, i.e., the number of unpaired electrons (N_{FOD}), of the considered molecular species by means of FT-DFT calculations. The N_{FOD} values obtained by FT-TPSS, FT-TPSS0, and FT-TPSSHH methods are presented in Table 1 for both the low- and high-spin states of all studied compounds. Complementarily, Figure 2 compares the calculated N_{FOD} values for the low-spin state of all compounds, from which we can recognize a close agreement between RAS-SF and FT-TPSS results. The results discussed along this section will thus limit to those obtained at the FT-TPSS level, with FT-TPSS0 slightly (FT-TPSSHH largely) overestimating the RAS-SF results. Moreover, all molecules present significant N_{FOD} values, indicating their open-shell (poly)radical character. The radical character is also preserved for the high-spin states, i.e. qualitatively similar N_{FOD}(LS) and N_{FOD}(HS) values are found except for Diradical I and II systems. Because fractional occupation is induced by near degeneracy, the smaller values of N_{FOD} for the HS state of Diradical I and II can be rationalized by their HOMO-1/HOMO and LUMO/LUMO+1 gaps, considerably larger than those of the other systems investigated. Interestingly, the series of [n]CPBM-Ant ($n = 3 - 6$) compounds is predicted to increase their radical character as a function of their increasing size, in perfect agreement with experimental and RAS-SF results.[53]

Following the agreement found between N_{FOD} values at the FT-TPSS and RAS-SF levels, see also Table S1, we represent in Figure 3 the topology (real-space distribution) of the corresponding density, $\rho^{FOD}(\mathbf{r})$, at the FT-TPSS level and using the recommended threshold[58,59] for the isocon-

tour values (σ = 0.005 e/bohr^3). For the Blatter-like radicals, the FOD density concentrates on the N atoms of the conjugated backbone, and on the nitrosyl substituents, in agreement with what one would expect from the resonance Lewis structures of the molecules. For 6CPPM-Mes, [n]CPBM-Ant ($n = 3 - 6$), and MC-F3A3 compounds we can observe how the FOD density locates mainly at those C atoms bringing the mesityl and anthracene substituents, respectively, acting effectively as protective synthons. For the 8MC compound we observe a delocalization of the FOD density on the non-bridging C atoms, resembling the results found for other systems with cyclic topologies as cyclacenes (i.e. cyclic oligoacenes[91]).

3.1.1 Radical(oid) indices.

In order to get a deeper insight into the radical nature of these compounds, in the following we explore them by means of their $\{y_i\}$ indices. Table 2 presents the y_0, y_1, y_2, and y_3 values for all the systems studied at the FT-TPSS level. The Blatter-like diradicals exhibit nearly ideal diradical character, with $y_0 \simeq 1.0$ and $y_{i>0} \simeq 0$ for the low and high-spin T_0 states. Note that this is in agreement with the smaller N_{FOD} values discussed in the previous section for the HS state of these two systems. The 6CPPM-Mes molecule holds a sizable tetraradicaloid character, with moderate y_0 and y_1 values for the ground-state singlet. For the [n]CPBM-Ant ($n = 3 - 6$) systems, we observe an increase of the number of strongly correlated electrons as a function of their size, in agreement with the trend found for the N_{FOD} values. Inspection of their y_i values allows to classify them as tri-, tetra-, penta- and hexaradicaloid molecules, respectively. Finally, for the 8MC molecule we obtain moderate values for all the y_{0-3} indices, indicating a moderate octaradicaloid behaviour. Tables S2-S3 present the y_i values ob-

tained at the FT-TPSS0 and FT-TPSSHH levels, respectively, which follow the same trend found for FT-TPSS, but with $\{y_i\}$ indices being systematically larger, like for N_{FOD} values.

3.2 Energy difference between low- and high-spin states.

Table 3 presents the energy difference $\Delta E(\mathrm{LS}-\mathrm{HS})$ between the low- and high-spin states of all the systems considered, calculated at the FT-TPSS, FT-TPSS0, and FT-TPSSHH levels. Note that, except for the Blatter-like diradicals considered, the electronic ground-state of these systems is always the one with the lowest spin-multiplicity, thus denoted as S_0 (singlet) or D_0 (doublet). Therefore, $\Delta E(\mathrm{LS}-\mathrm{HS})$ refers to the S_0-T_1 or D_0-Q_1 energy difference, respectively, and will hold a negative sign: $\Delta E(\mathrm{LS}-\mathrm{HS}) < 0$. For the Blatter-like diradicals, the triplet electronic ground-state is instead favoured, and in these cases it should be $\Delta E(\mathrm{LS}-\mathrm{HS}) > 0$ accordingly. First of all, inspecting the evolution of values in Table 3, we can see how the relative stabilization of the HS state with respect to the LS solution increases with the amount of Hartree-Fock exchange, i.e., upon going from FT-TPSS to FT-TPSS0, and to FT-TPSSHH, with the latter being systematically closer to experimental energy gaps. However, the agreement with experimental results largely differs among the set of compounds, even looking at the FT-TPSSHH results (i.e. best estimates) providing the lowest MSE and MUE values. For [6]CPBM or 8MC, employing any of the FT-DFT variants will lead to an error close or even less than 1 kcal/mol, commonly known as the chemical accuracy threshold. On the other hand, for [3]CPBM and MC-F3A3 compounds the computed gaps are a few kcal/mol too negative, even with the FT-TPSSH method. Figure 4 compares the FT-DFT calculated values with the experimental results, for which we can also easily

observe a different behaviour for odd and even [n]CPBM compounds. These facts, together with the spread of the results for MC-F3A3, allow us to conclude that the FT-DFT (with the default electronic temperatures) tends to overestimate the relative stability of low-spin (singlet or doublet) state with respect to the next higher spin state (triplet or quartet). Energy differences can be systematically improved, to some extend, by increasing the amount of exact exchange.

We compare next the SF-DFT and the experimental results in Table 4, also using the TPSS, TPSS0, and TPSSHH functionals to disclose the effect of linearly increasing the exact-exchange weight. First of all, we consider the FOD density as the criteria to select those atoms to flip, with the highest density localized on them, which could also be roughly estimated by inspecting the corresponding spin density. In this case, spin contamination becomes a key factor and results progressively deteriorates upon increasing the exact-exchange weight, contrarily to what happened with FT-DFT methods. The (spin-corrected) energy gaps $\Delta E(\mathrm{LS}-\mathrm{HS})$ keep an accuracy similar to that obtained for the uncorrected $\Delta E(\mathrm{BS}-\mathrm{HS})$ values, still with the SF-TPSS or SF-TPSS0 methods providing the closest agreement with experimental results (e.g., MUEs of 6.0 and 4.0–5.0 kcal/mol, respectively). Remarkably, the SF-TPSS method provides the correct lowest-energy spin-state for all the molecules considered, contrarily to SF-TPPS0 and especially SF-TPSSHH. Inspecting now the SF-TDDFT results in Table 5, done with the BHHLYP and thus comparable with TPSSHH in terms of having a similar exact exchange proportion, we observe larger averaged errors than for previous FT-DFT or SF-DFT methods, with a reverse state ordering for Diradicals I and II. The method yields too large energy differences for the

set of [n]CPBM compounds, but it keeps the correct trend of decreasing the ΔE values with increasing size.

For the sake of comparison of all these results, RAS-SF gives a MSE (MUE) of –0.55 (0.85) kcal/mol with respect to experimental results, with a maximum deviation of 3.2 kcal/mol and producing thus more accurate relative energies than the investigated DFT-based methods. Actually, this method is able to provide the chemical accuracy sought for the whole set of compounds. Discarding the case of [6]CPPM-Mes, the MSE (MUE) would decrease to –0.22 (0.56) kcal/mol, and thus being considerably low.

3.3 Zero-field splitting interactions

The magnetic dipole-dipole (i.e., spin-spin) interaction leads to the splitting of the triplet sublevels ($M_s = 0, \pm 1$) even in the absence of any external field; a physical effect described by the Zero-Field Splitting (ZFS) Hamiltonian:

$$\hat{H}_{ZFS} = \hat{\mathbf{S}} \cdot \hat{\mathbf{D}} \cdot \hat{\mathbf{S}} = D_{xx}\hat{S}_x^2 + D_{yy}\hat{S}_y^2 + D_{zz}\hat{S}_z^2 = D\left(\hat{S}_z^2 - \frac{1}{3}\hat{\mathbf{S}}^2\right) + E\left(\hat{S}_x^2 - \hat{S}_y^2\right), \tag{8}$$

with D_{ii} the principal values of the ZFS diagonal tensor $\hat{\mathbf{D}}$, which by convention are recasted as $D = D_{zz} - \frac{1}{2}(D_{xx} + D_{yy})$ and $E = \frac{1}{2}(D_{xx} - D_{yy})$. For systems having $S > 1/2$, the ZFS usually dominates the spectral shape of the Electron Paramagnetic Resonance (EPR) spectra, and thus the absolute values of D and the E/D ratio determine the energies of the three magnetic sublevels.[92] Additionally, provided that the point-dipole approximation holds, D also relates with the averaged distance (Δr) between ideally localized spin densities, and can be thus used to estimate the size of the photoexcited triplet exciton[93] (see the Supporting Information for further

details). Note that in the following we will restrict the study to those systems possessing ground-state or low-lying triplet states, i.e., with an even number of electrons.

First of all, we have thoroughly assessed the accuracy of DFT methods to calculate the D and E parameters for the pair of systems (Diradicals I and II) for which experimental measurements are available.[51] For both compounds it is clear that $D/hc < 0$ from the experimental EPR spectra, thus indicating a prolate-like distribution of the spin density for the triplet state. The sign of D indicates whether the $M_s = 0$ ($D > 0$) or $M_s = \pm 1$ ($D < 0$) spin substrates are the lowest energy states at zero external fields. However, previous results at the B3LYP/EPR-II level,[51] and with different exchange-correlation functionals and basis sets (see Tables S4-S5), predicted the wrong sign for Diradical II ($D/hc > 0$), which is properly characterized only by certain range-separated functionals (i.e., ωB97X-D[85] and LC-BLYP[94]) together with basis sets suited for electric and magnetic properties, i.e. IGLO-II or EPR-II, previously applied[95] to the study of spin-spin contributions to the ZFS tensor in organic radicals too.

This deficiency of DFT methods has also been documented before[96,97] and prompted us to apply in the following the ωB97X-D functional for consistency. Note also that the range-separated CAM-B3LYP functional[99] was also used but did not bring the correct sign of D for Diradical II. The main difference between the ωB97X-D/LC-BLYP and CAM-B3LYP schemes is a relatively large (35%) fixed DFT exchange contribution in the latter, and thus a maximum screened exact exchange of 65%, which seems to corroborate the importance of that variable part (80% and 100% for ωB97X-D

and LC-BLYP, respectively). On the other hand, looking again at Tables S4-S5, the relative error for the calculation of E was found larger than for D, in agreement with previous applications to heavy-atoms coordination complexes.[98]

Table 6 presents the D, E, and Δr calculated values (at the ωB97X-D/IGLO-II level) for the lowest triplet state of the set of compounds studied. Interestingly, for the Diradicals I and II, a high-spin ground-state together with a negative D could lead to effective molecular magnets.[13] In the case of 8MC, we can see how $E = 0$ due to the perfect axial symmetry of this compound, with E being considerably lower than D as expected in all other cases. Inspecting the Δr values, i.e., the mean inter-spin distance in a dipole-dipole approximation, see the Supporting Information for further details about the explicit derivation, we can see how it decreases with the system size; a fact also documented before for linear polyenes and polyacenes.[100] This is rationalized by the dependence $D \propto r^{-3}$ with r the distance between the spins of the unpaired electrons. We can also compare these results with the estimated exciton size (Δr) for the triplet ground-state of 2,6,10-Tri-*tert*-Butyltriangulene,[101] around 5.6 Å, or for the photoexcited triplet state of tetracene and pentacene,[102] around 3.8 Å, or for the photoexcited triplet state of B- and N-doped nanographenes,[103] around 4.4-5.2 Å depending on their size.

4 Conclusions

We report here a benchmark study of a set of real-world (poly)radicaloids, focusing on the extent of the radical character, spatial distribution of the

unpaired electrons, and singlet-triplet (or doublet-quartet) energy difference obtained with different electronic structure methods. Current research on organic (poly)radicaloid character and its applications has prompted the application here of both (cost-effective) DFT-based and RAS-SF methods, with the latter method behaving more accurately than the others as compared with reference experimental results. Complementarily, we have systematically compared finite-temperature (FT-DFT) and spin-flip approaches (SF-DFT and SF-TDDFT) with various exchange-correlation functionals, mostly differing in their exact exchange weight, to disentangle the effect of the underlying expression as well as the effect of the spin-contamination introduced. Evidently, the use of any of these approaches with a GGA form (i.e., TPSS) is less costly than using a hybrid expression. Finally, we have also calculated the ZFS parameters for the triplet states of the compounds, as well as their exciton size. Overall, we have shown how the cost-effective characterization of (poly)radicaloid nature in conjugated organic compounds is still a challenging issue, precluding the blind application of DFT variants.

Acknowledgements

G.S. acknowledges the Erasmus+ program for a research internship. D.C. is thankful to projects PIBA19-0004 (Eusko Jaurlaritza) and CTQ2016-80955-P from the Spanish Government (MINECO/FEDER).

Supplementary Material

The Supplementary Material contains in this order: (i) the metrics error used to compare the performance of the different methods; (ii) N_U and $\Delta E(\mathrm{LS}-\mathrm{HS})$ values obtained at the RAS-SF level for all the compounds;

(iii) calculated radical indices (y_i) at the FT-TPSS0 and FT-TPSSHH levels for all the compounds; (iv) comparison between calculated and experimental EPR parameters for Diradicals I and II; (v) notes on the theoretical estimates of the exciton size and the sign of the D-tensor; (vi) cartesian coordinates of all the compounds.

References

[1] Hu, X.; Wang, W.; Wang, D.; Zheng, Y. The electronic applications of stable diradicaloids: present and future. *Journal of Materials Chemistry C* **2018**, *6*, 11232–11242.

[2] Badía-Domínguez, I.; Pérez-Guardiola, A.; Sancho-García, J. C.; Lopez Navarrete, J. T.; Hernandez Jolin, V.; Li, H.; Sakamaki, D.; Seki, S.; Rúiz Delgado, M. C. Formation of Cyclophane Macrocycles in Carbazole-Based Biradicaloids: Impact of the Dicyanomethylene Substitution Position. *ACS Omega* **2019**, *4*, 4761–4769.

[3] Morita, Y.; Suzuki, S.; Sato, K.; Takui, T. Synthetic organic spin chemistry for structurally well-defined open-shell graphene fragments. *Nature chemistry* **2011**, *3*, 197.

[4] Pavliček, N.; Mistry, A.; Majzik, Z.; Moll, N.; Meyer, G.; Fox, D. J.; Gross, L. Synthesis and characterization of triangulene. *Nature Nanotechnology* **2017**, *12*, 308.

[5] Wang, S.; Talirz, L.; Pignedoli, C. A.; Feng, X.; Müllen, K.; Fasel, R.; Ruffieux, P. Giant edge state splitting at atomically precise graphene zigzag edges. *Nature Communications* **2016**, *7*, 11507.

[6] Li, J.; Sanz, S.; Corso, M.; Choi, D. J.; Peña, D.; Frederiksen, T.;

Pascual, J. I. Single spin localization and manipulation in graphene open-shell nanostructures. *Nature Communications* **2019**, *10*, 200.

[7] Pozo, I.; Majzik, Z.; Pavliček, N.; Melle-Franco, M.; Guitián, E.; Peña, D.; Gross, L.; Perez, D. Revisiting kekulene: synthesis and single-molecule imaging. *Journal of the American Chemical Society* **2019**, *141*, 15488–15493.

[8] Mondal, R.; Shah, B. K.; Neckers, D. C. Photogeneration of heptacene in a polymer matrix. *Journal of the American Chemical Society* **2006**, *128*, 9612–9613.

[9] Tönshoff, C.; Bettinger, H. F. Photogeneration of octacene and nonacene. *Angewandte Chemie International Edition* **2010**, *49*, 4125–4128.

[10] Segawa, Y.; Yagi, A.; Matsui, K.; Itami, K. Design and Synthesis of carbon nanotube segments. *Angewandte Chemie International Edition* **2016**, *55*, 5136–5158.

[11] Povie, G.; Segawa, Y.; Nishihara, T.; Miyauchi, Y.; Itami, K. Synthesis of a carbon nanobelt. *Science* **2017**, *356*, 172–175.

[12] Stuyver, T.; Chen, B.; Zeng, T.; Geerlings, P.; De Proft, F.; Hoffmann, R. Do Diradicals Behave Like Radicals? *Chemical Reviews* **2019**,

[13] Perumal, S.; Minaev, B.; Ågren, H. Spin-spin and spin-orbit interactions in nanographene fragments: A quantum chemistry approach. *The Journal of Chemical Physics* **2012**, *136*, 104702.

[14] Ortiz, R.; Boto, R. Á.; García-Martínez, N.; Sancho-García, J. C.;

Melle-Franco, M.; Fernández-Rossier, J. Exchange rules for diradical *pi*-conjugated hydrocarbons. *Nano Letters* **2019**, *19*, 5991–5997.

[15] Ovchinnikov, A. A. Multiplicity of the ground state of large alternant organic molecules with conjugated bonds. *Theoretica Chimica Acta* **1978**, *47*, 297–304.

[16] Lieb, E. H. Two theorems on the Hubbard model. *Physical Review Letters* **1989**, *62*, 1201.

[17] Das, A.; Muller, T.; Plasser, F.; Lischka, H. Polyradical Character of Triangular Non-Kekulé Structures, Zethrenes, p-Quinodimethane-Linked Bisphenalenyl, and the Clar Goblet in Comparison: An Extended Multireference Study. *The Journal of Physical Chemistry A* **2016**, *120*, 1625–1636.

[18] Hajgató, B.; Deleuze, M. S. Quenching of magnetism in hexagonal graphene nanoflakes by non-local electron correlation. *Chemical Physics Letters* **2012**, *553*, 6–10.

[19] Illas, F.; Moreira, I. P.; De Graaf, C.; Barone, V. Magnetic coupling in biradicals, binuclear complexes and wide-gap insulators: a survey of ab initio wave function and density functional theory approaches. *Theoretical Chemistry Accounts* **2000**, *104*, 265–272.

[20] Moscardó, F.; San-Fabián, E. Density-Functional Formalism and the Two-Body Problem. *Physical Review A* **1991**, *44*, 1549.

[21] Perdew, J. P.; Savin, A.; Burke, K. Escaping the Symmetry Dilemma through a Pair-Density Interpretation of Spin-Density Functional Theory. *Physical Review A* **1995**, *51*, 4531.

[22] Miehlich, B. B.; Stoll, H.; Savin, A. A Correlation-Energy Density Functional for Multideterminantal Wavefunctions. *Molecular Physics* **1997**, *91*, 527–536.

[23] Moscardó, F.; Pérez-Jiménez, A. J. Self-Consistent Field Calculations Using Two-Body Density Functionals for Correlation Energy Component: I. Atomic Systems. *Journal of Computational Chemistry* **1998**, *19*, 1887–1898.

[24] Moscardó, F.; Pérez-Jiménez, A. J.; Cjuno, J. A. Self-Consistent Field Calculations Using Two-Body Density Functionals for Correlation Energy Component: II. Small Molecules. *Journal of Computational Chemistry* **1998**, *19*, 1899–1908.

[25] McDouall, J. J. Combining Two-Body Density Functionals with Multiconfigurational Wavefunctions: Diatomic Molecules. *Molecular Physics* **2003**, *101*, 361–371.

[26] Sancho-García, J. C.; Moscardó, F. Usefulness of the Colle–Salvetti Model for the Treatment of the Nondynamic Correlation. *The Journal of Chemical Physics* **2003**, *118*, 1054–1058.

[27] Takeda, R.; Yamanaka, S.; Yamaguchi, K. Approximate On-Top Pair Density into One-Body Functions for CAS-DFT. *International Journal of Quantum Chemistry* **2004**, *96*, 463–473.

[28] Gusarov, S.; Malmqvist, P.-Å.; Lindh, R. Using On-Top Pair Density for Construction of Correlation Functionals for Multideterminant Wave Functions. *Molecular Physics* **2004**, *102*, 2207–2216.

[29] Toulouse, J.; Colonna, F.; Savin, A. Long-Range–Short-Range Sepa-

ration of the Electron-Electron Interaction in Density-Functional Theory. *Physical Review A* **2004**, *70*, 062505.

[30] Li Manni, G.; Carlson, R. K.; Luo, S.; Ma, D.; Olsen, J.; Truhlar, D. G.; Gagliardi, L. Multiconfiguration Pair-Density Functional Theory. *Journal of Chemical Theory and Computation* **2014**, *10*, 3669–3680.

[31] Gagliardi, L.; Truhlar, D. G.; Li Manni, G.; Carlson, R. K.; Hoyer, C. E.; Bao, J. L. Multiconfiguration Pair-Density Functional Theory: A New Way to Treat Strongly Correlated Systems. *Accounts of Chemical Research* **2016**, *50*, 66–73.

[32] Hoyer, C. E.; Ghosh, S.; Truhlar, D. G.; Gagliardi, L. Multiconfiguration Pair-Density Functional Theory is as Accurate as CASPT2 for Electronic Excitation. *The Journal of Physical Chemistry Letters* **2016**, *7*, 586–591.

[33] Ghosh, S.; Cramer, C. J.; Truhlar, D. G.; Gagliardi, L. Generalized-Active-Space Pair-Density Functional Theory: An Efficient Method to Study Large, Strongly Correlated, Conjugated Systems. *Chemical Science* **2017**, *8*, 2741–2750.

[34] Grimme, S.; Waletzke, M. A Combination of Kohn–Sham Density Functional Theory and Multi-Reference Configuration Interaction Methods. *The Journal of Chemical Physics* **1999**, *111*, 5645–5655.

[35] Gräfenstein, J.; Cremer, D. The Combination of Density Functional Theory with Multi-Configuration Methods–CAS-DFT. *Chemical Physics Letters* **2000**, *316*, 569–577.

[36] Nakata, K.; Ukai, T.; Yamanaka, S.; Takada, T.; Yamaguchi, K.

CASSCF Version of Density Functional Theory. *International Journal of Quantum Chemistry* **2006**, *106*, 3325–3333.

[37] Pijeau, S.; Hohenstein, E. G. Improved Complete Active Space Configuration Interaction Energies with a Simple Correction from Density Functional Theory. *Journal of Chemical Theory and Computation* **2017**, *13*, 1130–1146.

[38] Pérez-Jiménez, Á. J.; Pérez-Jordá, J. M.; Sancho-García, J. C. Combining Two-Body Density Correlation Functionals with Multiconfigurational Wave Functions Using Natural Orbitals and Occupation Numbers. *The Journal of Chemical Physics* **2007**, *127*, 104102.

[39] Piris, M.; Lopez, X.; Ruipérez, F.; Matxain, J.; Ugalde, J. A Natural Orbital Functional for Multiconfigurational States. *The Journal of Chemical Physics* **2011**, *134*, 164102.

[40] Piris, M.; Ugalde, J. M. Perspective on Natural Orbital Functional Theory. *International Journal of Quantum Chemistry* **2014**, *114*, 1169–1175.

[41] Filatov, M.; Shaik, S. A Spin-Restricted Ensemble-Referenced Kohn–Sham Method and its Application to Diradicaloid Situations. *Chemical Physics Letters* **1999**, *304*, 429–437.

[42] Kazaryan, A.; Heuver, J.; Filatov, M. Excitation Energies from Spin-Restricted Ensemble-Referenced Kohn–Sham Method: A State-Average Approach. *The Journal of Physical Chemistry A* **2008**, *112*, 12980–12988.

[43] Filatov, M. Spin-Restricted Ensemble-Referenced Kohn–Sham Method: Basic Principles and Application to Strongly Correlated

Ground and Excited States of Molecules. *Wiley Interdisciplinary Reviews: Computational Molecular Science* **2015**, *5*, 146–167.

[44] Ess, D. H.; Johnson, E. R.; Hu, X.; Yang, W. Singlet- Triplet Energy Gaps for Diradicals from Fractional-Spin Density-Functional Theory. *The Journal of Physical Chemistry A* **2010**, *115*, 76–83.

[45] Grimme, S. Towards First Principles Calculation of Electron Impact Mass Spectra of Molecules. *Angewandte Chemie International Edition* **2013**, *52*, 6306–6312.

[46] Chai, J.-D. Density Functional Theory with Fractional Orbital Occupations. *The Journal of Chemical Physics* **2012**, *136*, 154104.

[47] Shao, Y.; Head-Gordon, M.; Krylov, A. I. The spin–flip approach within time-dependent density functional theory: Theory and applications to diradicals. *The Journal of Chemical Physics* **2003**, *118*, 4807–4818.

[48] Wang, F.; Ziegler, T. Time-dependent density functional theory based on a noncollinear formulation of the exchange-correlation potential. *The Journal of Chemical Physics* **2004**, *121*, 12191–12196.

[49] Wang, F.; Ziegler, T. The performance of time-dependent density functional theory based on a noncollinear exchange-correlation potential in the calculations of excitation energies. *The Journal of Chemical Physics* **2005**, *122*, 074109.

[50] Gallagher, N. M.; Bauer, J. J.; Pink, M.; Rajca, S.; Rajca, A. High-spin organic diradical with robust stability. *Journal of the American Chemical Society* **2016**, *138*, 9377–9380.

[51] Gallagher, N.; Zhang, H.; Junghoefer, T.; Giangrisostomi, E.; Ovsyannikov, R.; Pink, M.; Rajca, S.; Casu, M. B.; Rajca, A. Thermally and magnetically robust triplet ground state diradical. *Journal of the American Chemical Society* **2019**, *141*, 4764–4774.

[52] Li, Z.; Gopalakrishna, T. Y.; Han, Y.; Gu, Y.; Yuan, L.; Zeng, W.; Casanova, D.; Wu, J. [6]Cyclo-para-phenylmethine: an analog of benzene showing global aromaticity and open-shell diradical character. *Journal of the American Chemical Society* **2019**, *141*, 16266–16270.

[53] Ni, Y.; Sandoval-Salinas, M. E.; Tanaka, T.; Phan, H.; Herng, T. S.; Gopalakrishna, T. Y.; Ding, J.; Osuka, A.; Casanova, D.; Wu, J. [*n*]Cyclo-para-biphenylmethine polyradicaloids: [*n*]annulene analogs and unusual valence tautomerization. *Chem* **2019**, *5*, 108–121.

[54] Lu, X.; Lee, S.; Hong, Y.; Phan, H.; Gopalakrishna, T. Y.; Herng, T. S.; Tanaka, T.; Sandoval-Salinas, M. E.; Zeng, W.; Ding, J.; Casanova, D.; Osuka, A.; Kim, D.; Wu, J. Fluorenyl based macrocyclic polyradicaloids. *Journal of the American Chemical Society* **2017**, *139*, 13173–13183.

[55] Liu, C.; Sandoval-Salinas, M. E.; Hong, Y.; Gopalakrishna, T. Y.; Phan, H.; Aratani, N.; Herng, T. S.; Ding, J.; Yamada, H.; Kim, D.; Casanova, D.; Wu, J. Macrocyclic polyradicaloids with unusual superring structure and global aromaticity. *Chem* **2018**, *4*, 1586–1595.

[56] Casanova, D.; Head-Gordon, M. Restricted active space spin-flip configuration interaction approach: theory, implementation and examples. *Physical Chemistry Chemical Physics* **2009**, *11*, 9779–9790.

[57] Lin, C.-Y.; Hui, K.; Chung, J.-H.; Chai, J.-D. Self-Consistent Determination of the Fictitious Temperature in Thermally-Assisted-

Occupation Density Functional Theory. *RSC Advances* **2017**, *7*, 50496–50507.

[58] Grimme, S.; Hansen, A. A practicable real-space measure and visualization of static electron-correlation effects. *Angewandte Chemie International Edition* **2015**, *54*, 12308–12313.

[59] Bauer, C. A.; Hansen, A.; Grimme, S. The fractional occupation number weighted density as a versatile analysis tool for molecules with a complicated electronic structure. *Chemistry-A European Journal* **2017**, *23*, 6150–6164.

[60] Head-Gordon, M. Characterizing unpaired electrons from the one-particle density matrix. *Chemical Physics Letters* **2003**, *372*, 508–511.

[61] Yeh, C.-N.; Chai, J.-D. Role of Kekulé and non-Kekulé structures in the radical character of alternant polycyclic aromatic hydrocarbons: a TAO-DFT study. *Scientific Reports* **2016**, *6*, 30562.

[62] Nakano, M.; Kishi, R.; Ohta, S.; Takahashi, H.; Kubo, T.; Kamada, K.; Ohta, K.; Botek, E.; Champagne, B. Relationship between third-order nonlinear optical properties and magnetic interactions in open-shell systems: a new paradigm for nonlinear optics. *Physical Review Letters* **2007**, *99*, 033001.

[63] Pérez-Guardiola, A.; Sandoval-Salinas, M. E.; Casanova, D.; San-Fabián, E.; Pérez-Jiménez, A.; Sancho-Garcia, J.-C. The role of topology in organic molecules: origin and comparison of the radical character in linear and cyclic oligoacenes and related oligomers. *Physical Chemistry Chemical Physics* **2018**, *20*, 7112–7124.

[64] Yamaguchi, K.; Fukui, H.; Fueno, T. Molecular orbital (MO) theory

for magnetically interacting organic compounds. Ab-initio MO calculations of the effective exchange integrals for cyclophane-type carbene dimers. *Chemistry Letters* **1986**, *15*, 625–628.

[65] Yamaguchi, K.; Takahara, Y.; Fueno, T.; Houk, K. N. Extended Hartree-Fock (EHF) theory of chemical reactions. *Theoretica Chimica Acta* **1988**, *73*, 337–364.

[66] Yamanaka, S.; Okumura, M.; Nakano, M.; Yamaguchi, K. EHF theory of chemical reactions Part 4. UNO CASSCF, UNO CASPT2 and R(U)HF coupled-cluster (CC) wavefunctions. *Journal of Molecular Structure: THEOCHEM* **1994**, *310*, 205–218.

[67] Rinkevicius, Z.; Vahtras, O.; Ågren, H. Spin-flip time dependent density functional theory applied to excited states with single, double, or mixed electron excitation character. *The Journal of Chemical Physics* **2010**, *133*, 114104.

[68] Canola, S.; Casado, J.; Negri, F. The double exciton state of conjugated chromophores with strong diradical character: insights from TDDFT calculations. *Physical Chemistry Chemical Physics* **2018**, *20*, 24227–24238.

[69] Canola, S.; Dai, Y.; Negri, F. The Low Lying Double-Exciton State of Conjugated Diradicals: Assessment of TDUDFT and Spin-Flip TDDFT Predictions. *Computation* **2019**, *7*, 68.

[70] Krylov, A. I. Spin-flip configuration interaction: an electronic structure model that is both variational and size-consistent. *Chemical Physics Letters* **2001**, *350*, 522–530.

[71] Krylov, A. I. Spin-flip equation-of-motion coupled-cluster electronic

structure method for a description of excited states, bond breaking, diradicals, and triradicals. *Accounts of Chemical Research* **2006**, *39*, 83–91.

[72] Casanova, D.; Krylov, A. I. *Physical Chemistry Chemical Physics*, 2020,DOI: 10.1039/C9CP06507E.

[73] Tao, J.; Perdew, J. P.; Staroverov, V. N.; Scuseria, G. E. Climbing the density functional ladder: Nonempirical meta–generalized gradient approximation designed for molecules and solids. *Physical Review Letters* **2003**, *91*, 146401.

[74] Staroverov, V. N.; Scuseria, G. E.; Tao, J.; Perdew, J. P. Comparative assessment of a new nonempirical density functional: Molecules and hydrogen-bonded complexes. *The Journal of Chemical Physics* **2003**, *119*, 12129–12137.

[75] Weigend, F.; Ahlrichs, R. Balanced basis sets of split valence, triple zeta valence and quadruple zeta valence quality for H to Rn: Design and assessment of accuracy. *Physical Chemistry Chemical Physics* **2005**, *7*, 3297–3305.

[76] Kossmann, S.; Neese, F. Comparison of two efficient approximate Hartee–Fock approaches. *Chemical Physics Letters* **2009**, *481*, 240–243.

[77] Weigend, F. Hartree–Fock exchange fitting basis sets for H to Rn. *Journal of Computational Chemistry* **2008**, *29*, 167–175.

[78] Pettersen, E. F.; Goddard, T. D.; Huang, C. C.; Couch, G. S.; Greenblatt, D. M.; Meng, E. C.; Ferrin, T. E. UCSF Chimera: A Visu-

alization System for Exploratory Research and Analysis. *Journal of Computational Chemistry* **2004**, *25*, 1605–1612.

[79] Neese, F. Software update: the ORCA program system, version 4.0. *Wiley Interdisciplinary Reviews: Computational Molecular Science* **2018**, *8*, e1327.

[80] Schmidt, M. W.; Baldridge, K. K.; Boatz, J. A.; Elbert, S. T.; Gordon, M. S.; Jensen, J. H.; Koseki, S.; Matsunaga, N.; Nguyen, K. A.; Su et al., S. General atomic and molecular electronic structure system. *Journal of Computational Chemistry* **1993**, *14*, 1347–1363.

[81] Becke, A. D. A new mixing of Hartree–Fock and local density-functional theories. *The Journal of Chemical Physics* **1993**, *98*, 1372–1377.

[82] Orms, N.; Krylov, A. I. Singlet–triplet energy gaps and the degree of diradical character in binuclear copper molecular magnets characterized by spin-flip density functional theory. *Physical Chemistry Chemical Physics* **2018**, *20*, 13127–13144.

[83] Bernard, Y. A.; Shao, Y.; Krylov, A. I. General formulation of spin-flip time-dependent density functional theory using non-collinear kernels: Theory, implementation, and benchmarks. *The Journal of Chemical Physics* **2012**, *136*, 204103.

[84] Shao et al., Y. Advances in molecular quantum chemistry contained in the Q-Chem 4 program package. *Molecular Physics* **2015**, *113*, 184–215.

[85] Chai, J.-D.; Head-Gordon, M. Long-range corrected hybrid density

functionals with damped atom–atom dispersion corrections. *Physical Chemistry Chemical Physics* **2008**, *10*, 6615–6620.

[86] Schindler, M.; Kutzelnigg, W. Theory of magnetic susceptibilities and NMR chemical shifts in terms of localized quantities. II. Application to some simple molecules. *The Journal of Chemical Physics* **1982**, *76*, 1919–1933.

[87] Jensen, F. Basis set convergence of nuclear magnetic shielding constants calculated by density functional methods. *Journal of Chemical Theory and Computation* **2008**, *4*, 719–727.

[88] Stoychev, G. L.; Auer, A. A.; Neese, F. Automatic generation of auxiliary basis sets. *Journal of Chemical Theory and Computation* **2017**, *13*, 554–562.

[89] Neese, F. Calculation of the zero-field splitting tensor on the basis of hybrid density functional and Hartree-Fock theory. *The Journal of Chemical Physics* **2007**, *127*, 164112.

[90] Jost, P.; van Wüllen, C. Why spin contamination is a major problem in the calculation of spin–spin coupling in triplet biradicals. *Physical Chemistry Chemical Physics* **2013**, *15*, 16426–16427.

[91] Pérez-Guardiola, A.; Ortiz-Cano, R.; Sandoval-Salinas, M. E.; Fernández-Rossier, J.; Casanova, D.; Pérez-Jiménez, A.; Sancho-Garcia, J.-C. From cyclic nanorings to single-walled carbon nanotubes: disclosing the evolution of their electronic structure with the help of theoretical methods. *Physical Chemistry Chemical Physics* **2019**, *21*, 2547–2557.

[92] Richert, S.; Tait, C. E.; Timmel, C. R. Delocalisation of photoexcited

triplet states probed by transient EPR and hyperfine spectroscopy. *Journal of Magnetic Resonance* **2017**, *280*, 103–116.

[93] Buta, M. C.; Toader, A. M.; Frecus, B.; Oprea, C. I.; Cimpoesu, F.; Ionita, G. Molecular and Supramolecular Interactions in Systems with Nitroxide-Based Radicals. *International Journal of Molecular Sciences* **2019**, *20*, 4733.

[94] Tawada, Y.; Tsuneda, T.; Yanagisawa, S.; Yanai, T.; Hirao, K. A long-range-corrected time-dependent density functional theory. *The Journal of Chemical Physics* **2004**, *120*, 8425–8433.

[95] Sinnecker, S.; Neese, F. Spin- Spin Contributions to the Zero-Field Splitting Tensor in Organic Triplets, Carbenes and Biradicals A Density Functional and Ab Initio Study. *The Journal of Physical Chemistry A* **2006**, *110*, 12267–12275.

[96] Perumal, S. S. Zero-field splitting of compact trimethylenemethane analogue radicals with density functional theory. *Chemical Physics Letters* **2011**, *501*, 608–611.

[97] Ye, S.; Neese, F. How do heavier halide ligands affect the signs and magnitudes of the zero-field splittings in halogenonickel (II) scorpionate complexes? A theoretical investigation coupled to ligand-field analysis. *Journal of Chemical Theory and Computation* **2012**, *8*, 2344–2351.

[98] Duboc, C.; Ganyushin, D.; Sivalingam, K.; Collomb, M.-N.; Neese, F. Systematic theoretical study of the zero-field splitting in coordination complexes of Mn (III). Density functional theory versus multireference wave function approaches. *The Journal of Physical Chemistry A* **2010**, *114*, 10750–10758.

[99] Yanai, T.; Tew, D. P.; Handy, N. C. A new hybrid exchange–correlation functional using the Coulomb-attenuating method (CAM-B3LYP). *Chemical Physics Letters* **2004**, *393*, 51–57.

[100] Ganyushin, D.; Gilka, N.; Taylor, P. R.; Marian, C. M.; Neese, F. The resolution of the identity approximation for calculations of spin-spin contribution to zero-field splitting parameters. *The Journal of Chemical Physics* **2010**, *132*, 144111.

[101] Inoue, J.; Fukui, K.; Kubo, T.; Nakazawa, S.; Sato, K.; Shiomi, D.; Morita, Y.; Yamamoto, K.; Takui, T.; Nakasuji, K. The first detection of a Clar's hydrocarbon, 2,6,10-tri-tert-butyltriangulene: a ground-state triplet of non-Kekulé polynuclear benzenoid hydrocarbon. *Journal of the American Chemical Society* **2001**, *123*, 12702–12703.

[102] Bayliss, S. L.; Chepelianskii, A. D.; Sepe, A.; Walker, B. J.; Ehrler, B.; Bruzek, M. J.; Anthony, J. E.; Greenham, N. C. Geminate and nongeminate recombination of triplet excitons formed by singlet fission. *Physical Review Letters* **2014**, *112*, 238701.

[103] Pershin, A.; Hall, D.; Lemaur, V.; Sancho-Garcia, J.-C.; Muccioli, L.; Zysman-Colman, E.; Beljonne, D.; Olivier, Y. Highly emissive excitons with reduced exchange energy in thermally activated delayed fluorescent molecules. *Nature Communications* **2019**, *10*, 597.

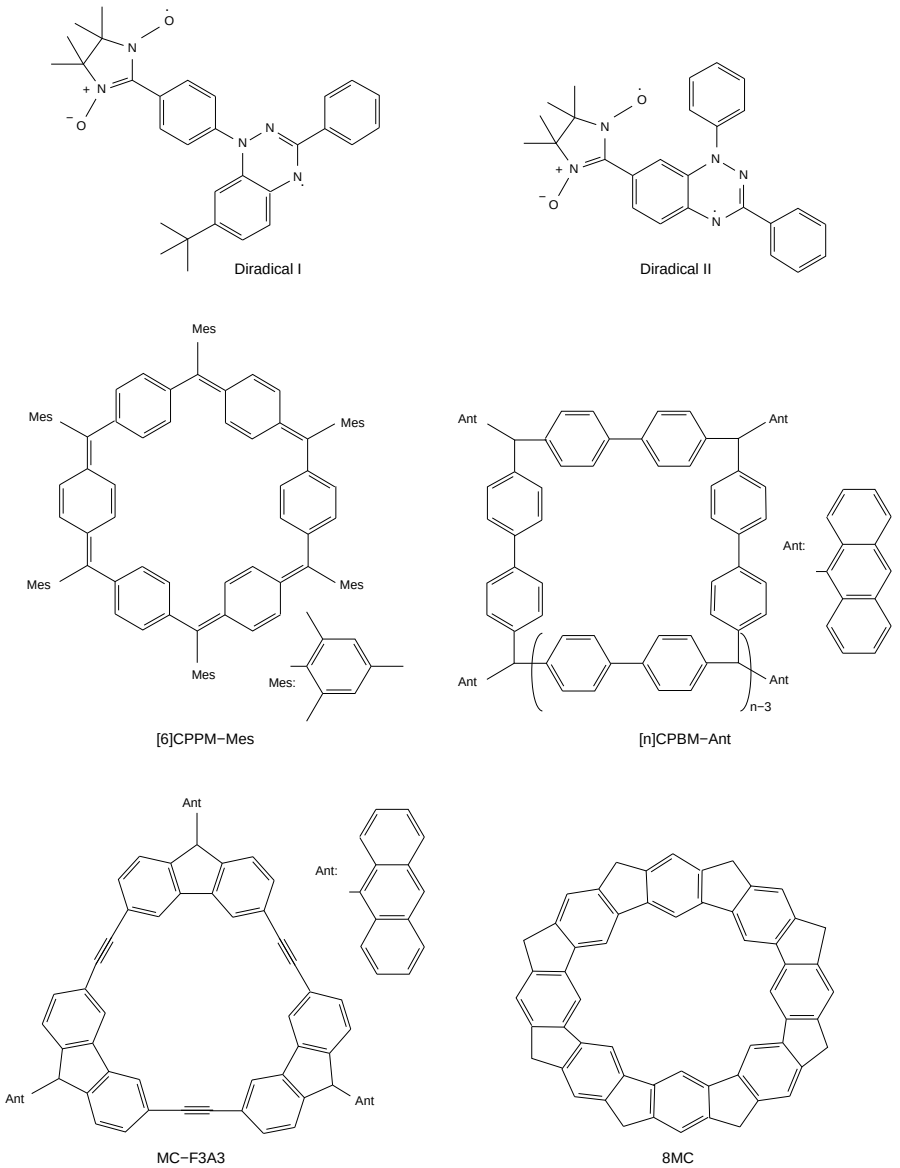

Figure 1: Chemical structures of the investigated compounds

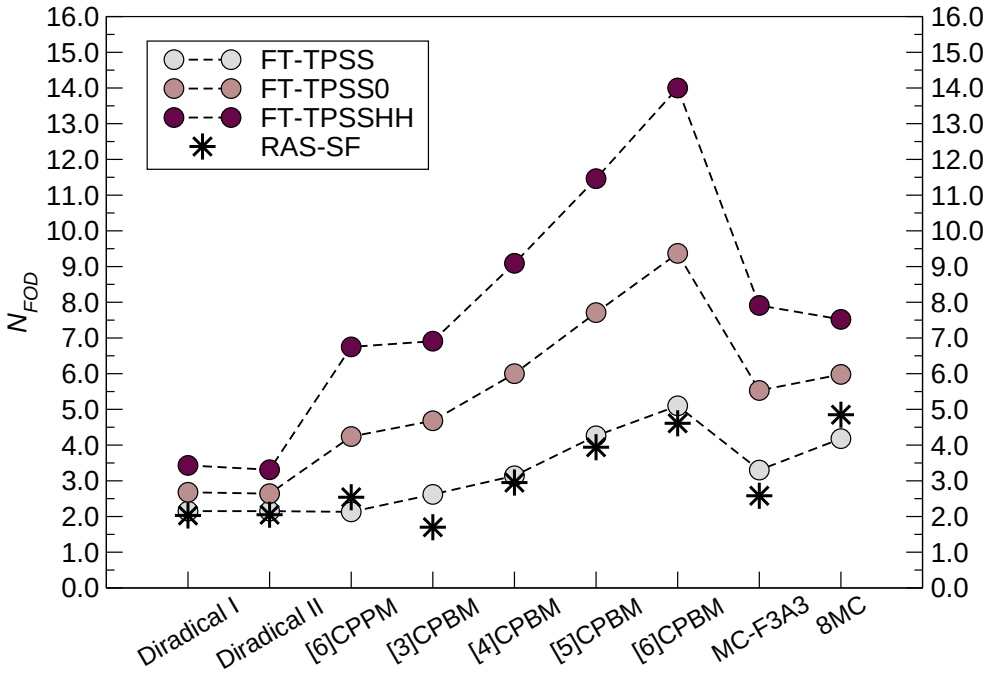

Figure 2: Comparison between FT-DFT and RAS-SF N_{FOD} values for the low-spin state of the set of studied compounds.

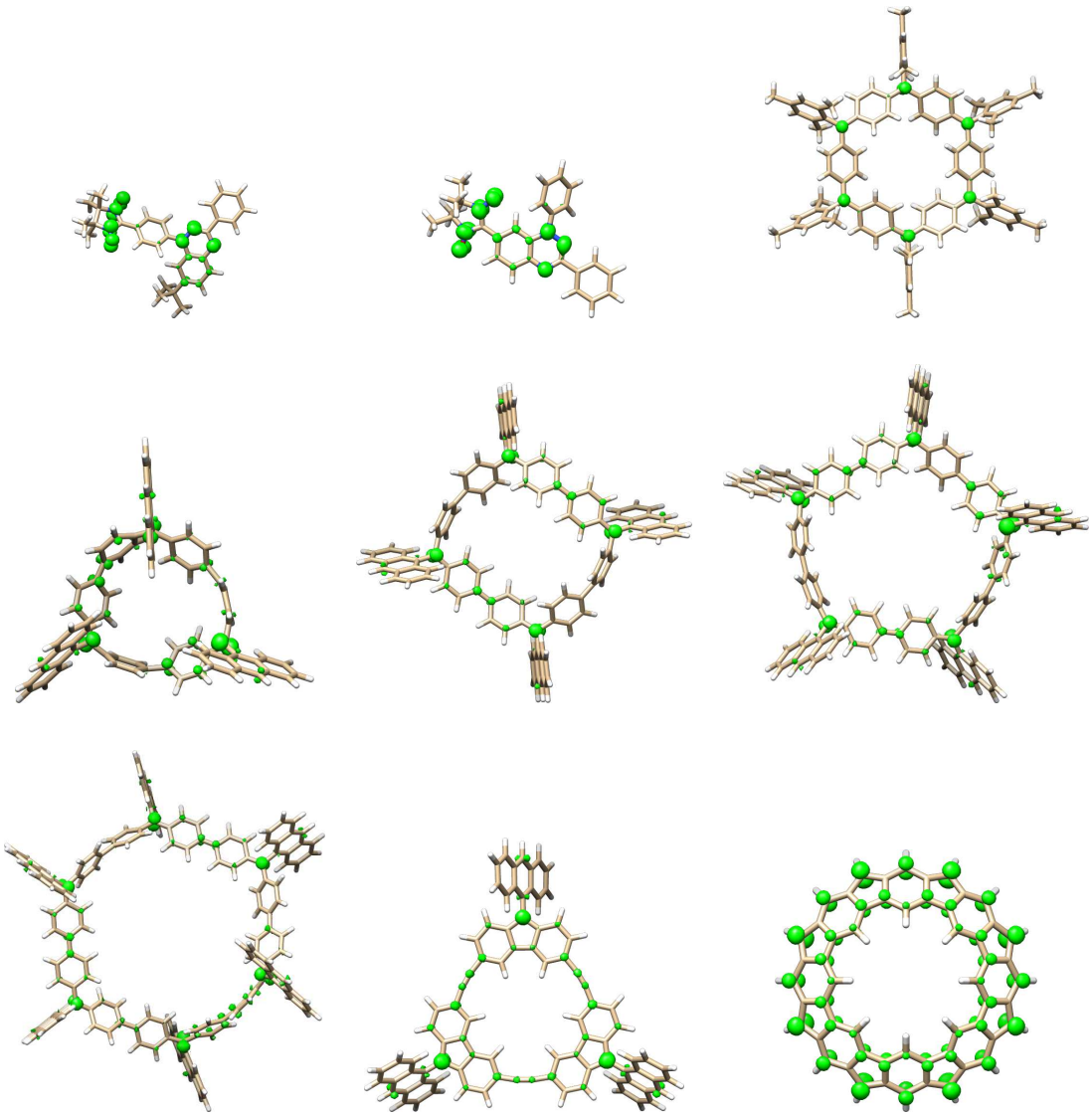

Figure 3: FOD density plots (σ = 0.005 e/bohr^3) obtained from the FT-TPSS/def2-TZVP method for the set of studied compounds.

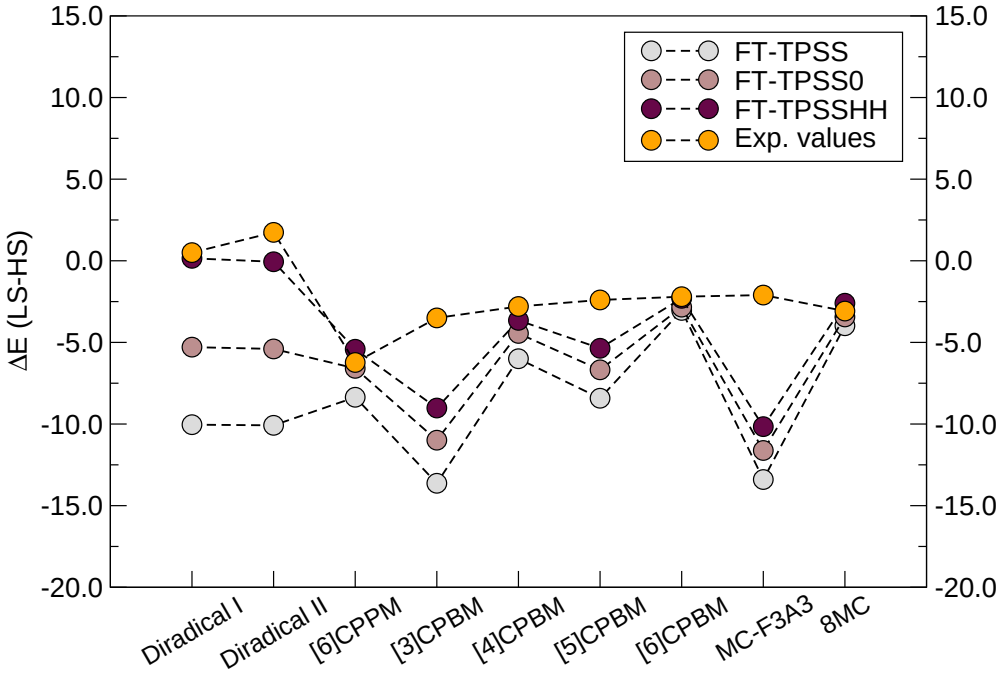

Figure 4: Comparison between $\Delta E(\mathrm{LS}-\mathrm{HS})$ (kcal/mol) computed (FT-DFT) and experimental values for the set of studied compounds.

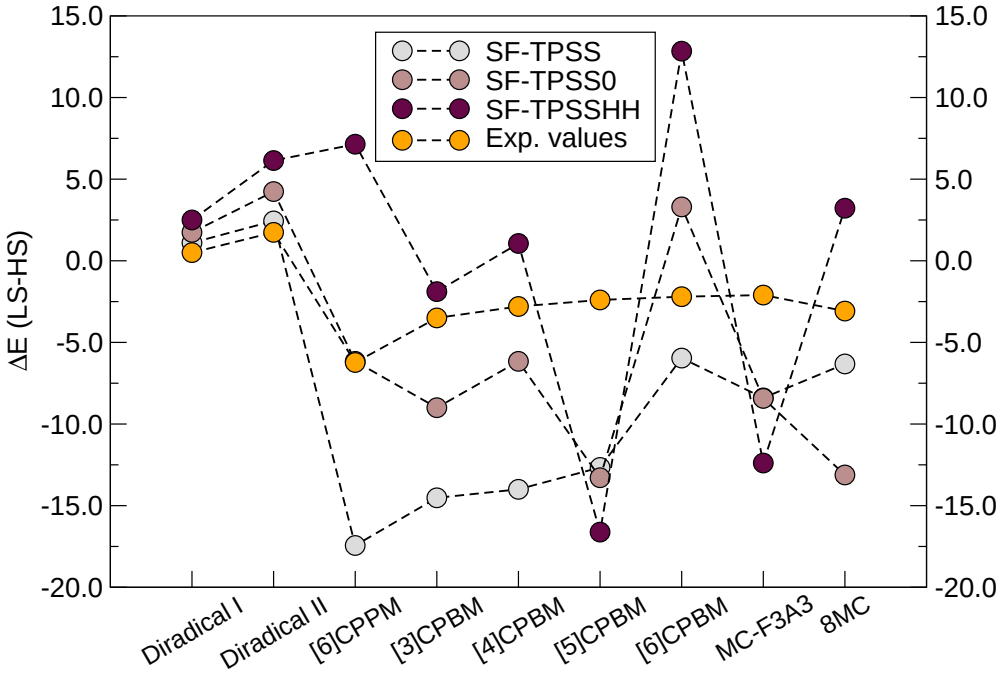

Figure 5: Comparison between $\Delta E(\mathrm{LS}-\mathrm{HS})$ (kcal/mol) computed (SF-DFT) and experimental values for the set of studied compounds.

Table 1: N_{FOD} values obtained at different theoretical levels.

		FT-TPSS		FT-TPSS0		FT-TPSSHH	
Compound	GS	N_{FOD}(LS)	N_{FOD}(HS)	N_{FOD}(LS)	N_{FOD}(HS)	N_{FOD}(LS)	N_{FOD}(HS)
Diradical I[a]	T_0	2.15	0.81	2.68	1.44	3.43	2.23
Diradical II[a]	T_0	2.15	0.79	2.64	1.42	3.31	2.10
[6]CPPM-Mes	S_0	2.13	2.90	4.24	4.82	6.75	7.24
[3]CPBM-Ant	D_0	2.62	2.78	4.68	4.78	6.91	6.99
[4]CPBM-Ant	S_0	3.14	3.70	6.00	6.43	9.09	9.44
[5]CPBM-Ant	D_0	4.26	4.61	7.71	7.95	11.46	11.66
[6]CPBM-Ant	S_0	5.10	5.50	9.37	9.63	14.00	14.17
MC-F3A3	D_0	3.30	3.13	5.53	5.37	7.91	7.73
8MC	S_0	4.18	4.34	5.98	5.93	7.52	7.36

[a] Note that for these systems the header classification do not apply, since the ground-state is already the T_0 and thus the HS state.

Table 2: Calculated radical indices (y_i^α) by the FT-DFT method at the TPSS/def2-TZVP level.

Compound	y_0^α	y_1^α	y_2^α	y_3^α
Diradical I	0.49	0.03	0.02	0.00
Diradical II	0.49	0.03	0.00	0.00
[6]CPPM-Mes	0.24	0.22	0.04	0.00
[3]CPBM-Ant	0.35	0.08	0.08	0.08
[4]CPBM-Ant	0.28	0.21	0.06	0.06
[5]CPBM-Ant	0.31	0.29	0.08	0.08
[6]CPBM-Ant	0.34	0.28	0.21	0.06
MC-F3A3	0.46	0.07	0.07	0.06
8MC	0.30	0.30	0.21	0.21

Table 3: Energy difference (kcal/mol) between the low-spin (LS) and high-spin (HS) states, $\Delta E(\mathrm{LS}-\mathrm{HS})$, obtained at the FT-DFT level.

Compound	GS	FT-TPSS	FT-TPSS0	FT-TPSSHH	Exp.
Diradical I	T_0	–10.04	–5.29	0.15	0.50±0.02
Diradical II	T_0	–10.08	–5.40	–0.06	1.74±0.07
[6]CPPM-Mes	S_0	–8.36	–6.50	–5.42	–6.23±0.78
[3]CPBM-Ant	D_0	–13.63	–10.99	–9.02	–3.5
[4]CPBM-Ant	S_0	–6.00	–4.45	–3.65	–2.8
[5]CPBM-Ant	D_0	–8.42	–6.68	–5.36	–2.4
[6]CPBM-Ant	S_0	–3.54	–2.84	–2.30	–2.2
MC-F3A3	D_0	–13.40	–11.62	–10.16	–2.10
8MC	S_0	–3.98	–3.44	–2.60	–3.08
	MSE	–6.4	–4.1	–2.0	
	MUE	6.4	4.1	2.3	
	MIN	0.9	0.4	0.4	
	MAX	11.8	9.5	8.1	

Table 4: Energy difference (kcal/mol) between the Broken-Symmetry (BS) and high-spin (HS) states, $\Delta E(\mathrm{BS}-\mathrm{HS})$, and the corresponding $\Delta E(\mathrm{LS}-\mathrm{HS})$ corrected, obtained at the SF-DFT level.

		SF-TPSS		SF-TPSS0		SF-TPSSHH		
Compound	GS	$\Delta E(\mathrm{BS}-\mathrm{HS})$	$\Delta E(\mathrm{LS}-\mathrm{HS})$	$\Delta E(\mathrm{BS}-\mathrm{HS})$	$\Delta E(\mathrm{LS}-\mathrm{HS})$	$\Delta E(\mathrm{BS}-\mathrm{HS})$	$\Delta E(\mathrm{LS}-\mathrm{HS})$	Exp.
Diradical I	T_0	0.55	1.10	0.88	1.74	1.32	2.50	0.50±0.02
Diradical II	T_0	1.23	2.44	2.18	4.24	3.34	6.14	1.74±0.07
[6]CPPM-Mes	S_0	–18.44	–17.44	–8.61	–6.16	12.94	7.14	–6.23±0.78
[3]CPBM-Ant	D_0	–14.61	–14.52	–9.21	–9.00	–2.05	–1.89	–3.5
[4]CPBM-Ant	S_0	–14.07	–14.00	–8.62	–6.16	1.27	1.06	–2.8
[5]CPBM-Ant	D_0	–12.60	–12.66	–10.16	–13.29	–11.41	–16.62	–2.4
[6]CPBM-Ant	S_0	–6.29	–5.96	3.48	3.30	15.85	12.84	–2.2
MC-F3A3	D_0	–7.89	–8.40	–5.97	–8.43	–7.47	–12.39	–2.10
8MC	S_0	–6.72	–6.32	–8.06	–13.12	1.93	3.22	–3.08
	MSE	–6.5	–6.2	–2.7	–3.0	4.0	2.4	
	MUE	6.5	6.5	4.1	5.0	7.2	7.9	
	MIN	0.0	0.6	0.4	0.1	0.8	1.6	
	MAX	12.2	11.2	7.8	10.9	19.2	15.0	

Table 5: Energy difference (kcal/mol) between the low-spin (LS) and high-spin (HS) states, $\Delta E(\mathrm{LS}-\mathrm{HS})$, obtained at the SF-TDDFT level.

Compound	GS	SF-TDBHHLYP	Exp.
Diradical I	T_0	–9.34	0.50±0.02
Diradical II	T_0	–9.94	1.74±0.07
[6]CPPM-Mes	S_0	–3.37	–6.23±0.78
[3]CPBM-Ant	D_0	–17.99	—3.5
[4]CPBM-Ant	S_0	–17.80	–2.8
[5]CPBM-Ant	D_0	–15.86	–2.4
[6]CPBM-Ant	S_0	–9.34	–2.2
MC-F3A3	D_0	–6.69	—2.10
8MC	S_0	–0.57	–3.08
	MSE	–7.9	
	MUE	9.1	
	MIN	2.5	
	MAX	15.0	

Table 6: Calculated D and E EPR parameters (D/hc and E/hc in $10^3 cm^{-1}$) and exciton size (Δr, in Å)at the ωB97X-D/IGLO-II level, of the lowest triplet state of the selected compounds.

Compound	D	E	Δr
Diradical I	–5.52	–0.80	7.8
Diradical II	–11.13	–3.66	6.2
[6]CPPM-Mes	–12.60	–0.56	5.9
[4]CPBM-Ant	–13.04	–1.74	5.8
[6]CPBM-Ant	–10.05	–0.04	6.4
8MC	4.29	0.00	8.5